Electronic Supplementary Material (ESI) for Journal of Materials Chemistry B.

Supporting information for

Continuous phase regulation of $MoSe_2$ from 2H to 1T for the optimization of peroxidase-like catalysis

Daomeng Liu,† Daquan Wang,† Xunan Jing,† Xiaoping Zhao,† Duo Xi,† Dongfeng Dang,† and Lingjie Meng*,†,‡

†School of Science; MOE Key Laboratory for Nonequilibrium Synthesis and Modulation of Condensed Matter; Xi'an Key Laboratory of Sustainable Energy Material Chemistry; Xi'an Jiaotong University, Xi'an 710049, P. R. China.

‡Instrumental Analysis Center of Xi'an Jiaotong University, Xi'an 710049, P. R. China.

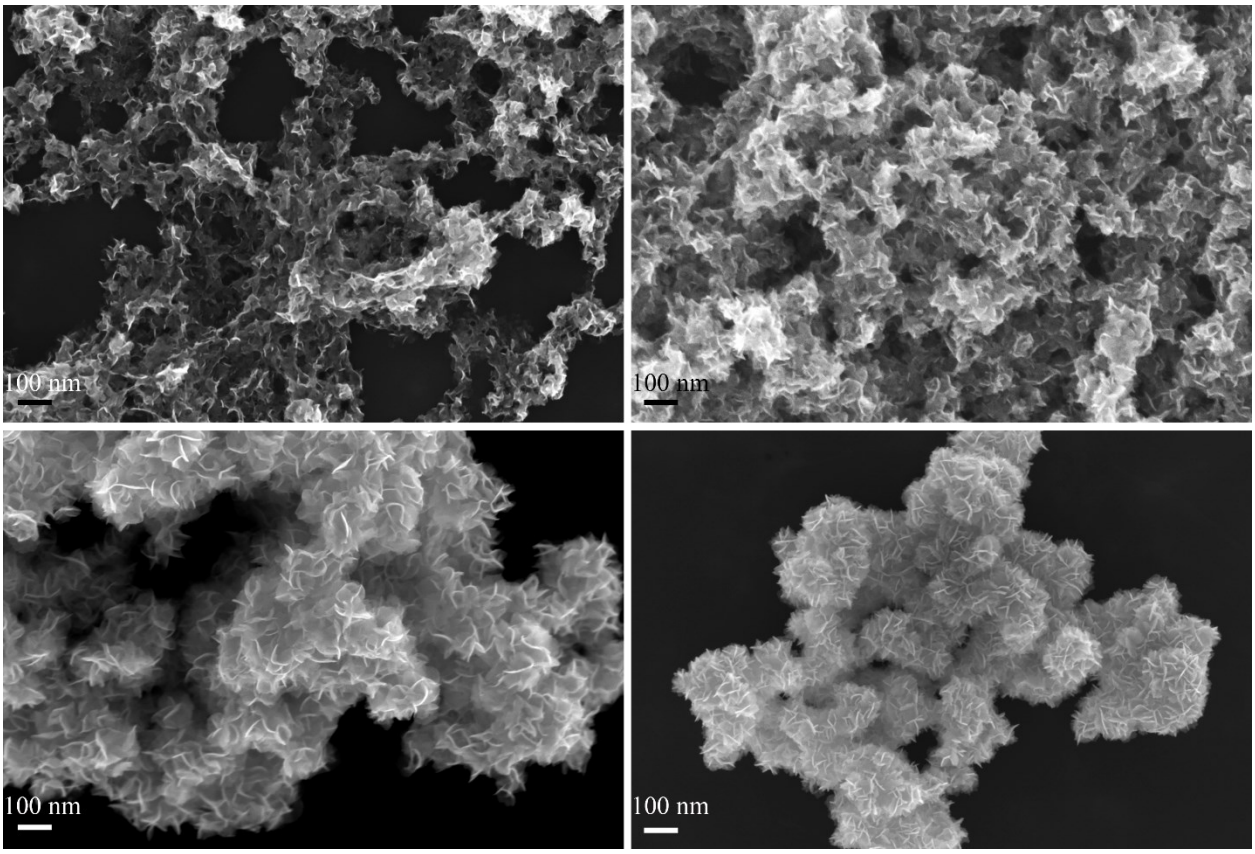

Figure S1 SEM images at different reaction temperatures. (a) $MoSe_2$–180, (b) $MoSe_2$–200, (c) $MoSe_2$–220, (d) $MoSe_2$–240.

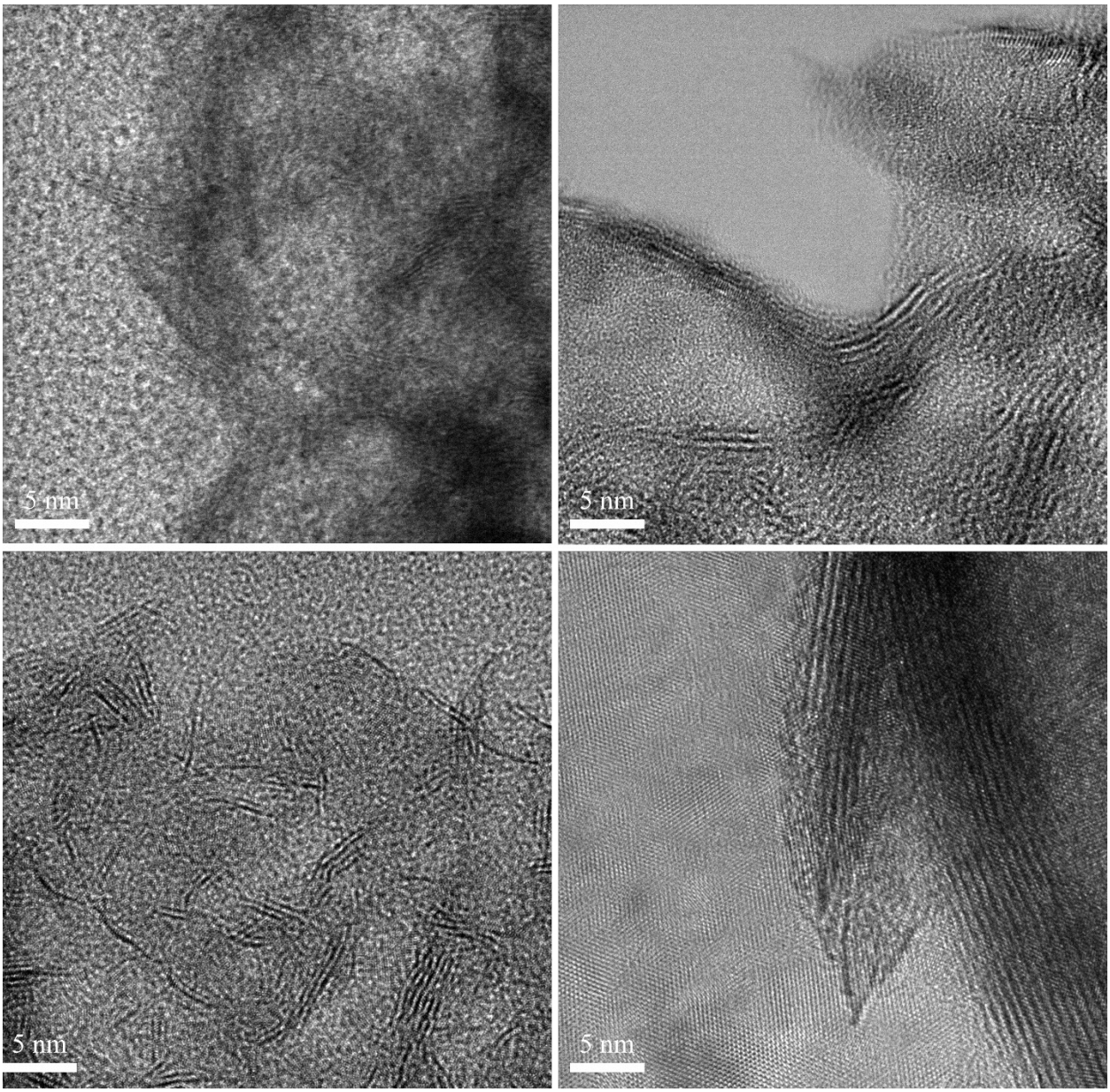

Figure S2 HRTEM images at different reaction temperatures. (a) $MoSe_2$–180, (b) $MoSe_2$–200, (c) $MoSe_2$–220, (d) $MoSe_2$–240.

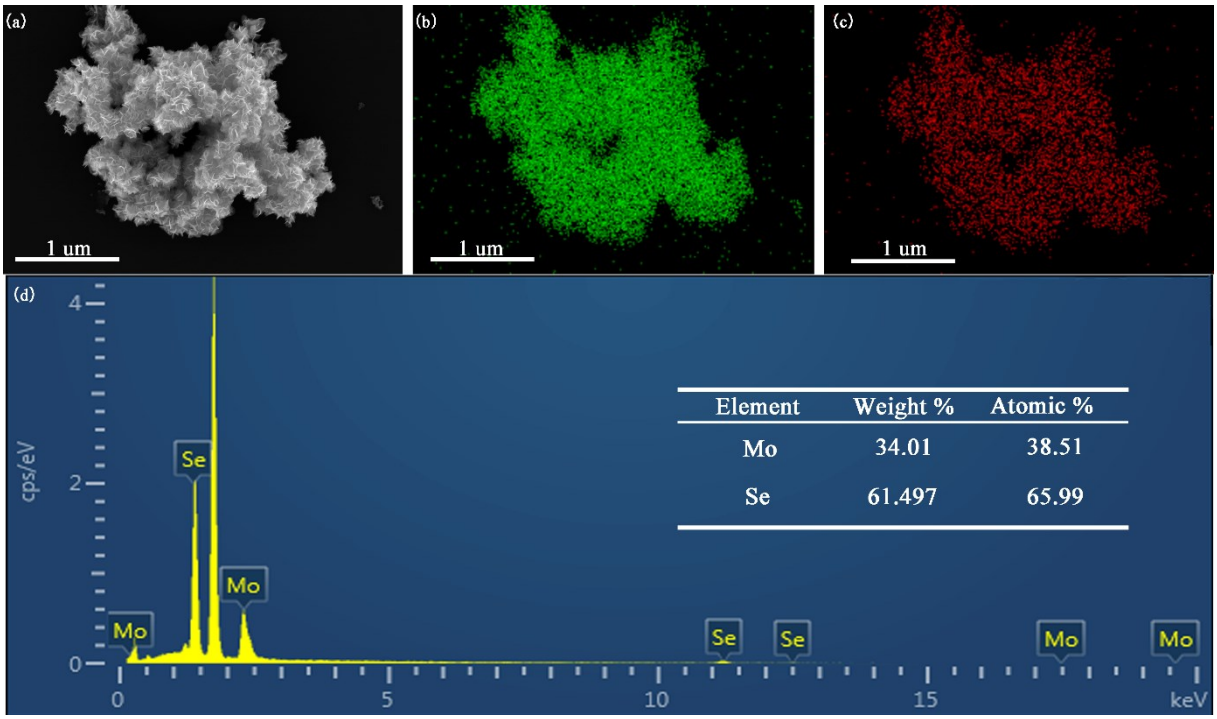

Figure S3 Energy-dispersive X-ray spectroscopy (EDS) of $MoSe_2$-220.

Table S1 the phase content for various $MoSe_2$ samples

Phase Content	Samples			
	$MoSe_2$-180	$MoSe_2$-200	$MoSe_2$-220	$MoSe_2$-240
1T	76.57%	57.48%	45.73%	10.40%
2H	23.43%	42.52%	54.27%	89.60%

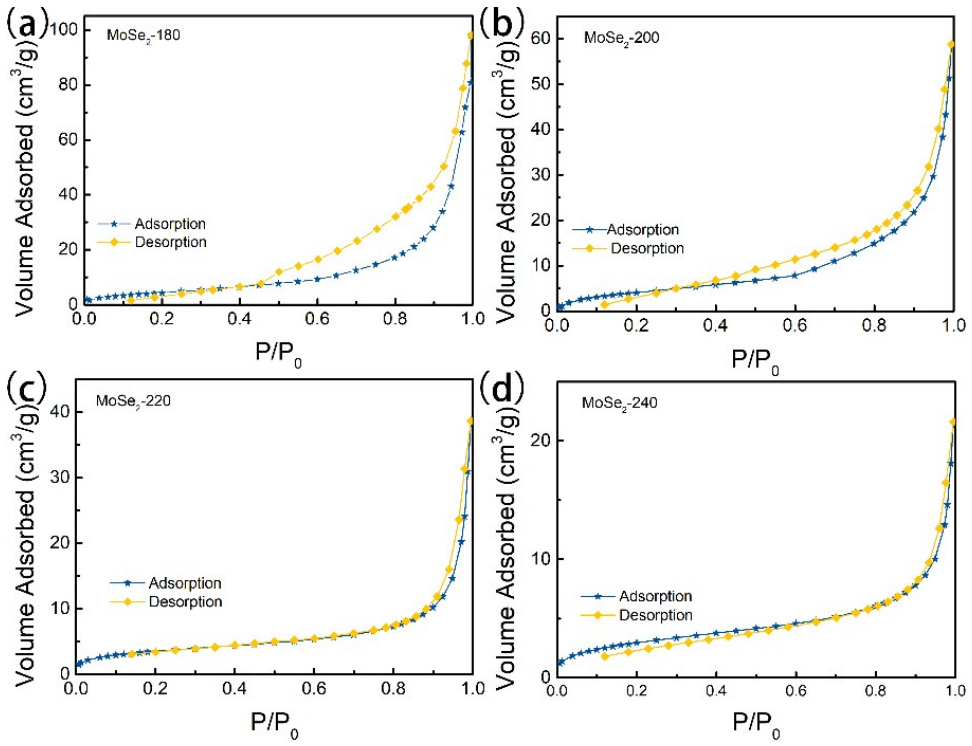

Figure S4 Nitrogen adsorption-desorption isothermals of (a) $MoSe_2$-180, (b) $MoSe_2$-200, (c) $MoSe_2$-220, (b) $MoSe_2$-240.

The nitrogen adsorption-desorption isotherm curves of $MoSe_2$-T nanostructures were measured (Figure S4). All the samples showed type III isotherms and H3 hysteresis rings, indicating the existence of rich gaps among the nanosheets. The specific surface areas of the four samples were calculated by BET method as follows, $MoSe_2$-180 (17.52 $m^2 \cdot g^{-1}$), $MoSe_2$-200 (16.41 $m^2 \cdot g^{-1}$), $MoSe_2$-220 (12.69 $m^2 \cdot g^{-1}$) and $MoSe_2$-240 (11.01 $m^2 \cdot g^{-1}$). With the increase of reaction temperature, the BET surface areas decreased gradually. Whereas, $MoSe_2$-220 with relatively smaller BET surface area exhibited the best catalytic activity, indicating the mixing 1T/2H phase (~1:1) could provide more active sites on a unit BET surface.

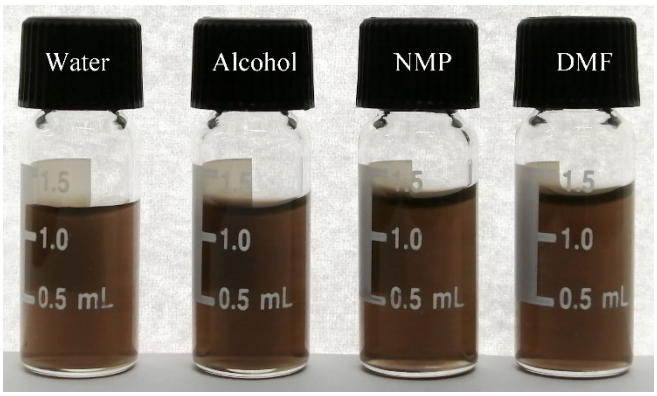

Figure S5. Stability of CHI-$MoSe_2$-220 in various solvents. Solvents from left to right: water, alcohol, N-methyl-pyrrolidone (NMP), and N, N-dimethyl formamide (DMF), respectively. All the dispersions were stored for at least 48 hours before taking photos.

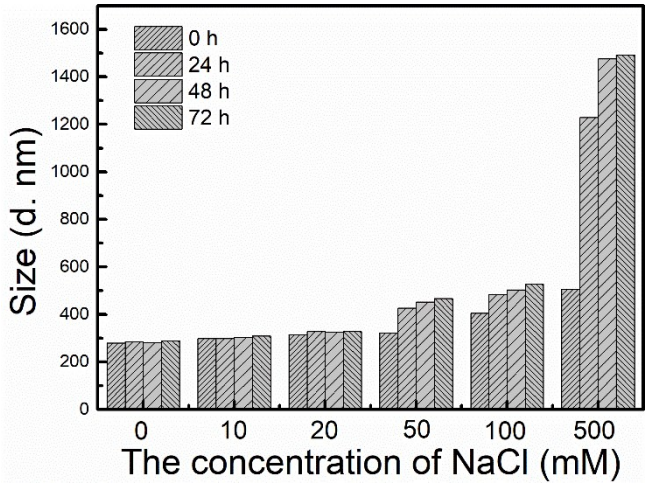

Figure S6 Stability of CHI-$MoSe_2$-220 in sodium chloride salt solution.

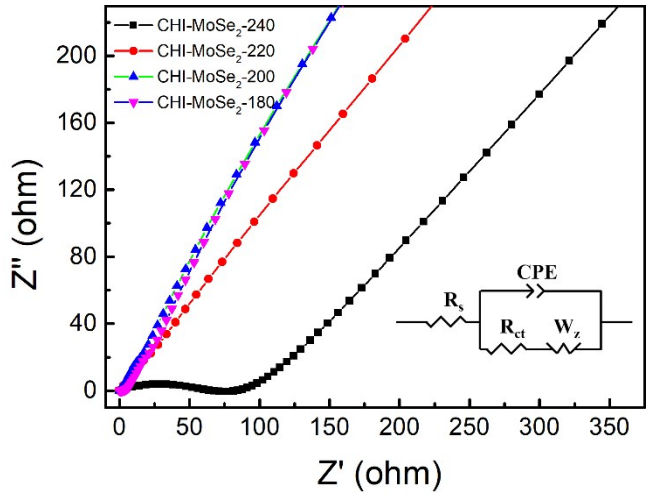

Figure S7 Nyquist plots of different samples and the equivalent circuit model. The electrochemical impedance spectroscopies (EIS) further reveal similar system resistance for all the tested electrodes and low charge-transfer resistance for the nanostructured CHI-$MoSe_2$-T.

Table S2 Impedance parameters derived using equivalent circuit model for the as-prepared samples

Samples	R_s	R_{ct}
CHI-$MoSe_2$-180	124.3	59.78
CHI-$MoSe_2$-200	134.3	63.56
CHI-$MoSe_2$-220	135.8	53.26
CHI-$MoSe_2$-240	126.4	129.0

Electrochemical Measurements: Electrochemical measurements were performed in a three-electrode system at an electrochemical station (CHI660B). Using Ag/AgCl (in 3.5 M KCl solution) as the reference electrode, platinum foil as the counter electrode, and glassy carbon electrode coated with drop cast CHI-$MoSe_2$-T catalysts as the working electrode. The catalyst was ultrasonically dispersed in a water-ethanol solution (v/v 3:1), and a drop of the catalyst (5 μL, 0.5 mg mL^{-1}) was then transferred onto the glassy carbon electrode with a geometric

area of 0.07 cm^2. The amount of deposited catalyst was calculated to be 10 μg, namely an estimated catalyst loading of 0.04 mg cm^2. The electrochemical impedance spectroscopy (EIS) measurements were carried out at 250 mV overpotential in the frequency range from 10 6 to 0.1 Hz.

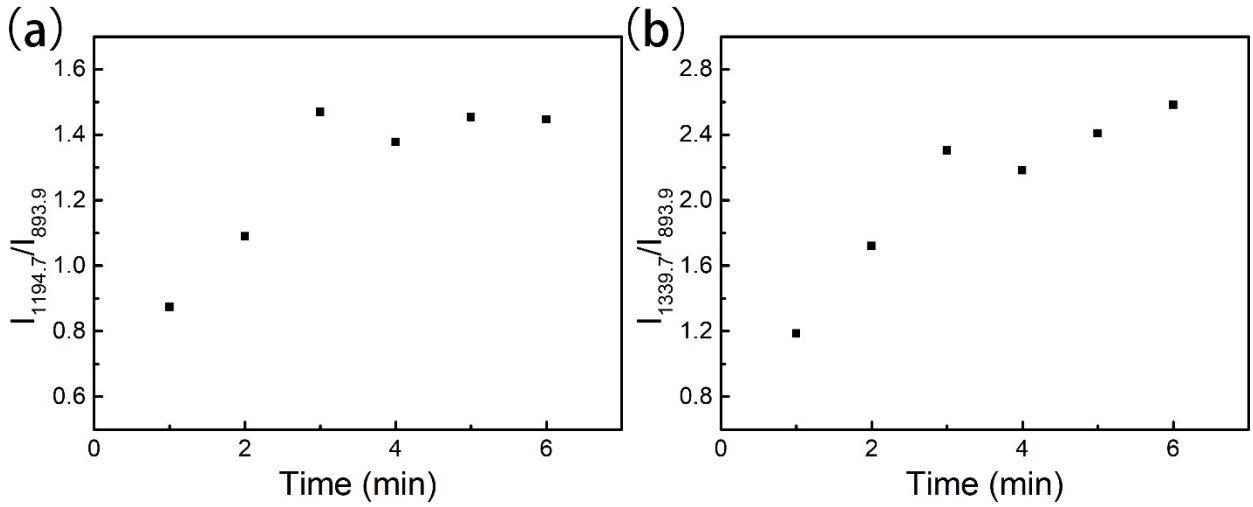

Figure S8 Linear relationship between the time and relative intensity of the situ Raman spectrum bands at (a) 1194.7 cm^{-1} and (b) 1339.7 cm^{-1} for oxidized TMB.

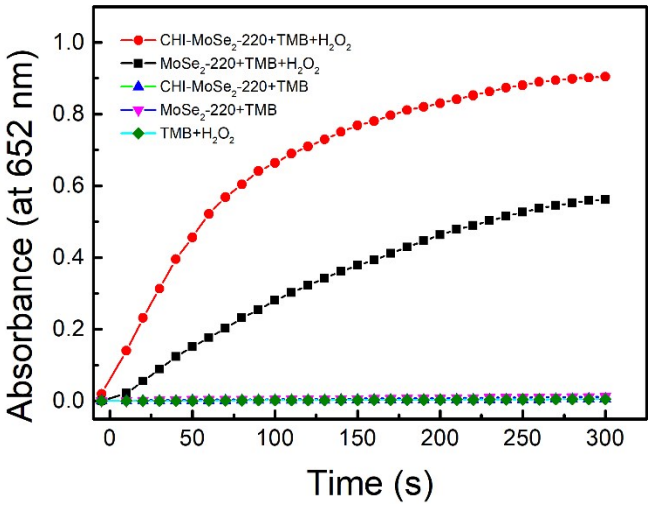

Figure S9. Time-dependent absorbance at 652 nm in different reaction systems. In all experiments were performed at acetate buffer (0.2 M, pH 3.5), NFs, TMB and H_2O_2 concentrations of 20 μg mL^{-1}, 0.5 mM and 100 mM, respectively.

Table S3 Comparison of the kinetic parameters of HPR, WSe_2 NFs, GO-COOH, MoS_2 NFs, WS_2 NFs, $MoSe_2$-220 and CHI-$MoSe_2$-220.

Catalyst	substrate	Km (mM)	Vmax (10^{-8} M S^{-1})	Ref.
HPR	TMB	0.43	10.00	1
	H_2O_2	3.70	8.71	
WSe_2 NFs	TMB	0.04	1.43	2
	H_2O_2	19.53	2.22	
GO-COOH	TMB	0.02	3.45	3
	H_2O_2	3.99	3.85	
MoS_2 NFs	TMB	0.53	5.16	4
	H_2O_2	0.01	4.29	
WS_2 NFs	TMB	1.83	4.31	5
	H_2O_2	0.24	4.52	
$MoSe_2$-220	TMB	0.04	7.90	This work
	H_2O_2	19.45	2.98	
CHI-$MoSe_2$-220	TMB	0.02	8.15	This work
	H_2O_2	0.94	3.05	

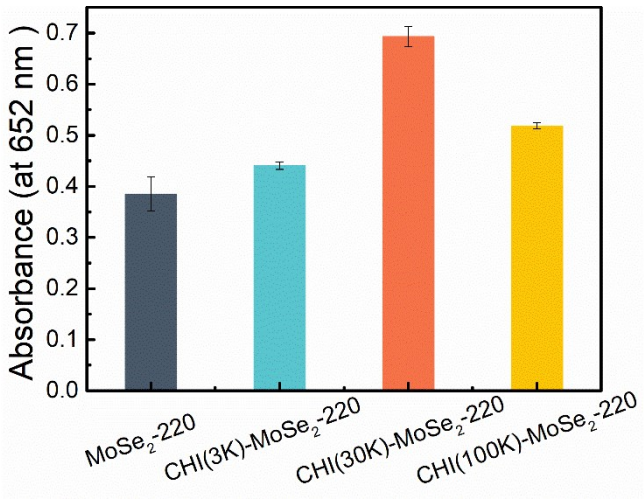

Figure S10 Effect of molecular weight of chitosan on $MoSe_2$-220 peroxidase-like activity

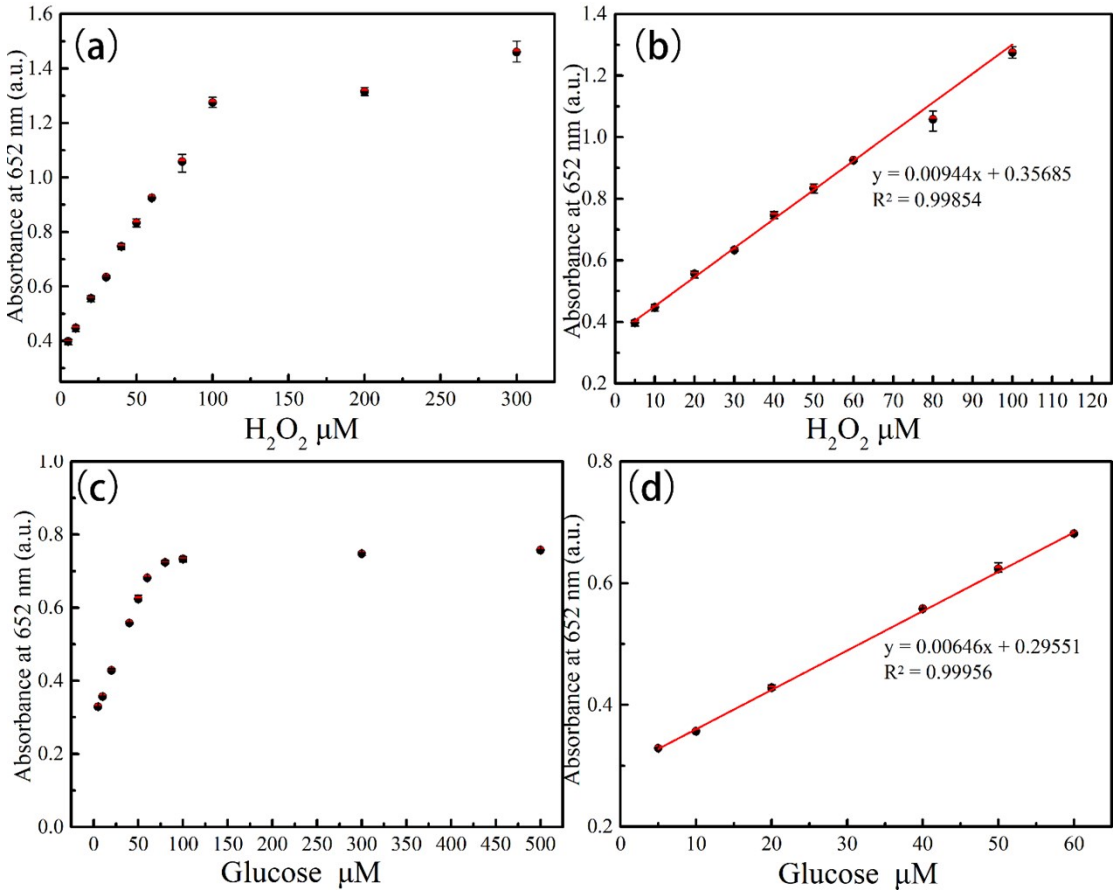

Figure S11 H_2O_2 and glucose sensing based on nanozymes. The concentration-response curve of H_2O_2 (a) and glucose (c) detection using CHI-$MoSe_2$-220 as a peroxidase-like enzyme, and a linear calibration chart of H_2O_2 (b) and glucose (d). All tests were performed under optimal reaction conditions. Error bars represent the standard deviation of the three measurements.

Table S4 Comparison of various materials for detection of H_2O_2 and glucose include MoS_2 nanosheets, WS_2 nanosheets, SDS–MoS_2 NPs, MoS_2–$Pt_{74}Ag_{26}$, and CHI-$MoSe_2$-220.

System	LOD (μM)		Linear range (μM)		Ref.
	H_2O_2	glucose	H_2O_2	glucose	
MoS_2 nanosheets	1.50	1.20	5-100	5-150	4
WS_2 nanosheets	1.20	2.90	10-100	5-300	5
SDS–MoS_2 NPs	0.32	0.57	2-100	5-500	6
MoS_2–$Pt_{74}Ag_{26}$	0.40	0.80	1-50	1-10	7
CHI-$MoSe_2$-220	0.52	0.71	5-100	5-60	This work

Table S5 Results of determination of glucose in serum samples.

Sample	Glucose meter method (mM)[a]	Proposed method (mM)[b]	RSD%
Serum 1	6.46	6.25 ± 0.14	2%
Serum 2	7.20	7.09 ± 0.06	1%
Serum 3	4.53	4.42 ± 0.07	1%

[a] The glucose determination was performed directly without dilution in the laboratory for clinical analysis, the Affiliated Hospital of Xi'an JiaoTong University. [b] n=3

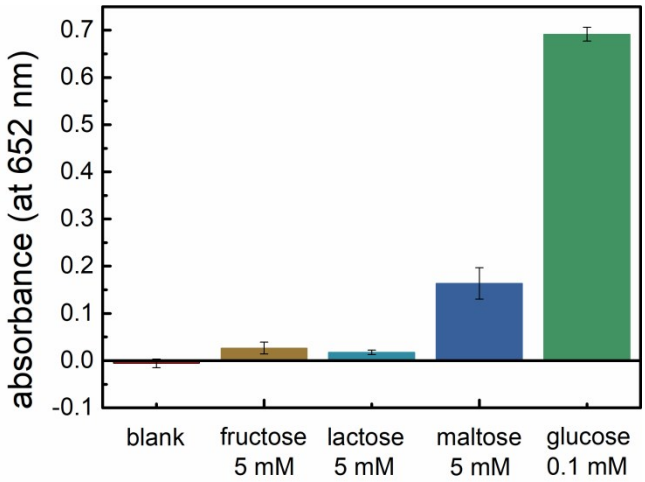

Figure S12 Selectivity analysis for glucose detection by monitoring the relative absorbance. The error bars represent the standard deviation of three measurements.

REFERENCE

1. L. Z. Gao, J. Zhuang, L. Nie, J. B. Zhang, Y. Zhang, N. Gu, T. H. Wang, J. Feng, D. L. Yang, S. Perrett and X. Yan, *Nature Nanotechnology*, 2007, **2**, 577-583.
2. T. M. Chen, X. J. Wu, J. X. Wang and G. W. Yang, *Nanoscale*, 2017, **9**, 11806-11813.
3. Y. Song, K. Qu, C. Zhao, J. Ren and X. Qu, *Advanced Materials*, 2010, **22**, 2206-2210.
4. T. Lin, L. Zhong, L. Guo, F. Fu and G. Chen, *Nanoscale*, 2014, **6**, 11856-11862.
5. T. R. Lin, L. S. Zhong, Z. P. Song, L. Q. Guo, H. Y. Wu, Q. Q. Guo, Y. Chen, F. F. Fu and G. N. Chen, *Biosens. Bioelectron.*, 2014, **62**, 302-307.
6. K. Zhao, W. Gu, S. S. Zheng, C. L. Zhang and Y. Z. Xian, *Talanta*, 2015, **141**, 47-52.
7. S. F. Cai, Q. S. Han, C. Qi, Z. Lian, X. H. Jia, R. Yang and C. Wang, *Nanoscale*, 2016, **8**, 3685-3693.